ISSN (Print) 1226-1750
ISSN (Online) 2233-6656
Journal of Magnetics 30(4), 672-680 (2025) https://doi.org/10.4283/JMAG.2025.30.4.672

Multi-Objective Optimization and Analysis of Thrust on an Axial Magnetized Dual Stator 2DoFPM Machine Linear Component

Hepeng Jia, Peixin Wang*, Yanqi Wei, Shuai Xu, Rui Nie, and Jikai Si

School of Electrical and Information Engineering, Zhengzhou University, Zhengzhou 450000, China

(Received 4 August 2025, Received in final form 4 December 2025, Accepted 9 December 2025)

Two degrees-of-freedom permanent magnet (2DoFPM) machines, which have high theoretical and practical value, are widely used in advanced manufacturing fields such as robotics and machine tools. This paper focuses on significant force ripples in the linear component of 2DoFPM machines and explores multi-objective optimization related to the output thrust of the linear component. First, on the basis of a theoretical analysis, the structure and operating principle of the 2DoFPM machine are briefly presented. Second, Taguchi's orthogonal array method is employed to design a simulation experiment. Third, three-dimensional finite element analysis (3D-FEA) of the machine is conducted. Last, through statistical analysis and data comparison, the optimal parameter combination is obtained.

Keywords : two-degrees-of-freedom permanent magnet machine, multi-objective optimization, Taguchi's orthogonal array method, finite element analysis

1. Introduction

Traditional mechanical transmission structures, which typically employ multiple single-degree-of-freedom machines, often face issues such as complex configurations and inconvenient maintenance because of these machines. However, 2DoFPM machines eliminate the need for intermediate transmission structures and can achieve multiple motion modes, including linear, rotational, and helical movements [1]. Therefore, owing to their flexibility and precision, 2DoFPM machines are widely used in the fields of robotics, automation, and machine tools [2].

Scholars have recently proposed and investigated various types of 2DoF machines, including induction machines [3-5], switched reluctance machines [6-8], and permanent magnet (PM) machines. PM motors have been the focus of numerous studies in the field of 2DoF machines because of their simple structure, high efficiency, and high reliability [9].

2DoFPM machines can be classified into two types: single-stator structure and double-stator structures. With respect to the single-stator structure, the rotary winding and linear winding share a common stator core. Owing to the coupling effect, the magnetic fields of the two motions interact, which results in higher requirements on control strategies. Additionally, the core saturation becomes more distinct, which requires more in-depth optimization methods to mitigate this effect [10]. With respect to the double-stator structure, because the two stators are physically separated, the coupling effect can be significantly reduced. A double-stator 2DoFPM machine was designed and analyzed, the nearly identical force and torque performance under helical motion and single-degree-of-freedom motion, confirm that the operating magnetic fields of the double-stator motor are decoupled, and that the two motions can be controlled by separate stators [9].

However, the double-stator structure also has potential drawbacks. For example, the inner-outer double-stator-type 2DoFPM machine [11, 12] has a three-layer structure: the innermost layer is the rotary stator, the middle layer is a mover composed of a PM array, and the outermost layer is the linear stator. Notable characteristics of this design include its large size, high usage of PMs, potential heat dissipation issues, and demagnetization risks. Consequently, its manufacturing process is both demanding and costly. Therefore, the 2DoFPM machine designed in this paper is an outer double-stator with axially magnetized PMs. The distinct advantages of the

*Corresponding author: Tel: +86-18300604205
e-mail: wangpeixin@zzu.edu.cn

machine are the outer arrangement of the stators, which facilitates heat dissipation, a simpler structure and smaller volume. Furthermore, the mover is composed of alternately arranged PMs and mover cores, which reduces PM usage and decreases manufacturing costs.

With respect to optimization, given the complex operating principle and multi-parameter nature of the motor, single-variable, single-objective optimization can improve performance but fails to improve overall performance because of the lack of analysis of parameter interactions [13, 14].

To achieve multi-objective optimal motor design, optimization algorithms such as the equivalent magnetic circuit method, genetic algorithm (GA), particle swarm optimization (PSO), and Taguchi method are now widely used. These methods are based on FEA results and are combined with optimization algorithms to summarize general optimization design criteria [15-18]. The Taguchi method is a practical and efficient robust optimization approach for multi-objective optimal motor design. This approach can determine the optimal parameter combination with minimal experimental trials, achieving multi-objective performance optimization [19-21]. There are also hybrid methods that combine the Taguchi method, improved differential evolution algorithm, and Pareto evaluation for motor optimization, which can accurately and effectively improve motor performance [22]. The Taguchi method facilitates rapid motor optimization with high design precision and has been widely applied in motor optimization recently.

In this paper, a dual-stator, axially magnetized 2DoFPM machine is investigated, with the aim of optimizing the force ripple-related performance of the decoupled linear component through multi-objective optimization. First, the topological structure and working principle of the machine are presented. Second, an experimental plan for simulation is designed on the basis of the Taguchi orthogonal method. Third, a three-dimensional finite element model is established to perform simulations and statistical analysis of data on the thrust of the linear component. Last, the data are analyzed to derive several parameter optimization schemes, and the feasibility of each optimized scheme is validated through simulation results.

2. Structure and Principle

2.1. Topology Structure and Dimensions

The topological structure of the 2DoFPM machine designed in this study is shown in Fig. 1. The structure consists of two upper and lower arc-shaped stators and a mover with protruding teeth in the circumferential direction. One type of stator, the rotary stator, is composed of axially arranged iron cores with small teeth that are uniformly distributed along the inner circumference of the stator poles, as shown in Fig. 1(a). The linear stator is composed of circumferentially arranged iron cores, with end teeth at both ends and a total of 7 slots, all of which are open-slot type, as shown in Fig. 1(b). The mover, which is composed of axially alternately arranged iron cores and PMs, is shown in Fig. 1(c). Small teeth are uniformly distributed on the outer circumference of the iron cores, and adjacent mover iron core teeth are staggered relative to each other. The motor consists of the linear stator, rotary stator, and mover, as shown in Fig. 1(d).

The following Table 1 lists the main design parameters of the preliminary 6-slot, 7-pole linear part of the machine. Subsequently, the model will be optimized through FEA based on the parameter table.

2.2. Operation Principle

The primary objective of this paper is to conduct an optimization analysis on the linear component of the 2DoFPM machine. Therefore, this section only brief discusses the principle of the rotary component; a detailed explanation of the linear component is provided in a subsequent section.

The rotary component of the 2DoFPM machine operates in accordance with the unified theory of air-gap magnetic field modulation for machines. As shown in the machine topology in Fig. 1, both the surface of the iron core of the mover and the poles of the rotary stator are equipped with slotted structures (also known as toothed structures). Slotting on both sides of the rotary stator and

Table 1. 2DoFPM machine dimension parameters.

Parameter	Unit	Value
Stator Inner and Outer Diameter	mm	20.6, 38
Permanent Magnet Inner and Outer Diameter	mm	7, 18
Mover Inner and Outer Diameter	mm	7, 19
Air-gap	mm	0.5
Mover Tooth Height	mm	1
Stator Tooth Width	mm	16
Slot Pitch	mm	20
Pole Pitch	mm	17.14
Permanent Magnet Width	mm	2.1
Mover Core Width	mm	15
Mover Length	mm	188.54
Mover Operating Speed	m/s	1.714

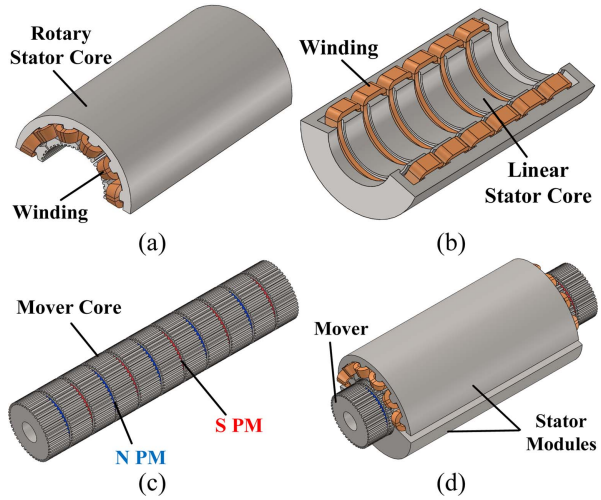

Fig. 1. (Color online) 2DoFPM machine model. (a) Rotary stator. (b) Linear stator. (c) Mover. (d) Assembly view.

mover enables modulation of the air-gap PM field and armature reaction field, resulting in rich harmonic content. Moreover, the modulated armature magnetic field contains harmonics of the same order as those in the PM field. On this basis, the motor can generate stable electromagnetic torque [10, 23].

The linear component of the 2DoFPM machine can be considered an extended form of a cylindrical linear motor. The principle of PM linear motors is highly similar to that of synchronous rotary motors, with the key difference being that the air-gap magnetic field undergoes translational motion rather than rotational motion. This air-gap magnetic field is also referred to as a traveling wave magnetic field. As shown in Fig. 2, when three-phase alternating current is supplied to the windings, a traveling wave magnetic field with speed v_s is generated in the air-gap. Through the interaction between this field and the field produced by the PMs and iron core of the mover, an electromagnetic thrust is generated, driving the mover to perform linear motion along the axial direction at speed v, which is equal to the speed of the traveling wave magnetic field. Within the entire machine system, an electromagnetic force acting in the same direction as the motion of the mover propels the mover. The mover supplies mechanical power, whereas the stator draws electrical power from the power grid.

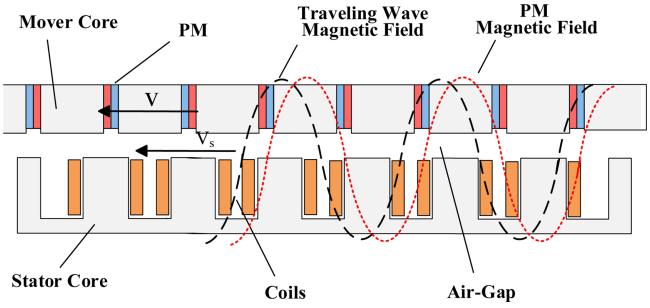

Fig. 2. (Color online) Operating principle of linear machine.

Therefore, it can be said that the two types of stators in the machine perform distinct functions: the rotary stator generates a rotating magnetic field, which, in conjunction with the salient pole teeth of the mover core and the PMs, generates rotary torque. Meanwhile, the linear stator generates a traveling wave magnetic field, which, in coordination with the iron core of the mover and axially alternately arranged PMs, generates linear thrust. Collectively, the mover of this machine can produce complex motion modes, including rotational motion, linear motion, and helical motion.

2.3. 3D Finite Element Model

To conduct optimization analysis on the decoupled linear component of the 2DoFPM machine, this study constructs a 3D-FEM of the 2DoFPM machine based on the electromagnetic simulation software Infolytica Magnet. The mesh model and the static PM field distribution of the model are shown in Fig. 3.

Fig. 3(a) presents the details of the mesh discretization of the model. Overall, the mesh division of the machine model is relatively fine, with additional refinement implemented in the air-gap region to more accurately simulate actual operating conditions. Additionally, as shown in Fig. 3(b), in the static PM flux distribution diagram, saturation only occurs at the edges of the mover salient teeth, while there is almost no saturation in other regions.

3. Multi-Objective Optimization Design

3.1. Taguchi Method Optimization

The Taguchi method, founded by Dr. Genichi Taguchi from Japan, is a quality engineering approach based on low cost and high efficiency. The optimization process of

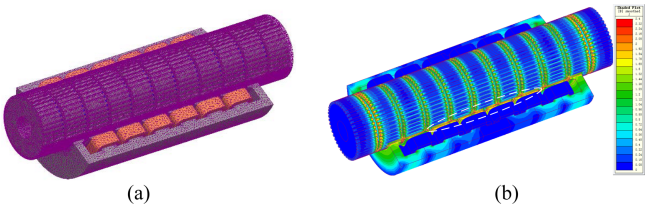

Fig. 3. (Color online) 3D finite element model of 2DoFPM machine. (a) Meshed model. (b) Static magnetic field distribution.

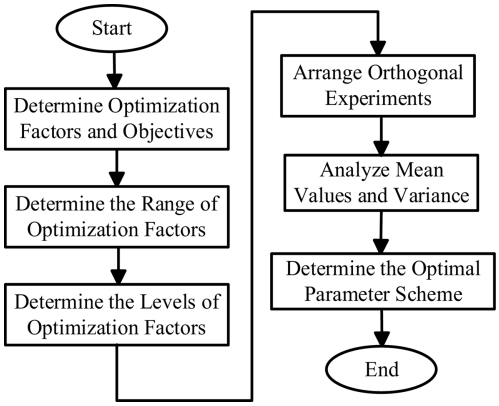

Fig. 4. Optimization process of the Taguchi method.

the Taguchi method is shown in Fig. 4.

The Taguchi method emphasizes that the improvement in product quality or optimization of performance is not achieved through inspection, but through design. This method uses orthogonal arrays to arrange experimental designs and identifies the most significant factors affecting the experimental objectives through statistical analysis of the results. The optimization plan for each factor is adjusted on the basis of the level of significance.

3.2. Optimization Factors and Objectives

The optimization objectives include thrust F_x, force ripple R_f, and the thrust-to-mass ratio of the PM R_{fp}. The latter is included because the cost of PMs accounts for a considerable portion of the total manufacturing cost in motor production. Therefore, the thrust-to-mass ratio of the PM is defined as a key metric to evaluate material efficiency.

The design parameters selected for analysis are the stator tooth width w_s, PM width w_p, air-gap thickness t_g, and stator yoke height t_y. A preliminary sensitivity analysis is conducted on these four factors. Based on the basic dimensions of the motor, the ranges and level values for each factor are defined in Tables 2 and 3.

Table 2. Range of design factors.

Factor	w_s/mm	w_p/mm	t_g/mm	t_y/mm
Lower Limit	6.5	2.0	0.35	5.0
Upper Limit	8.5	2.4	0.55	7.0

Table 3. Levels of design factors.

Factor	w_s/mm	w_p/mm	t_g/mm	t_y/mm
Level 1	6.5	2.0	0.35	5.0
Level 2	7.0	2.1	0.40	5.5
Level 3	7.5	2.2	0.45	6.0
Level 4	8.0	2.3	0.50	6.5
Level 5	8.5	2.4	0.55	7.0

Table 4. Factor influence degree.

Factor	Proportion/%		
	F_x	R_f	R_{fp}
w_s	1.87	55.32	0.92
w_p	84.91	24.19	93.95
t_g	10.68	12.75	3.94
t_y	2.54	7.74	1.19

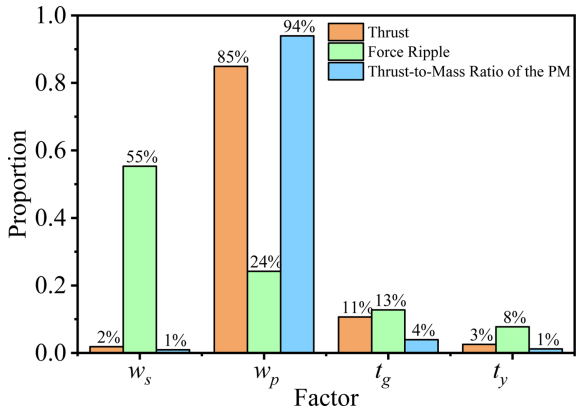

Fig. 5. (Color online) Comparison of the impact degree of four factors.

The influence of the four factors on the three objectives is assessed via 2D FEA, with results given in Table 4. As shown in Fig. 5, the stator tooth width, PM width, and air-gap thickness significantly affect the objectives, while the stator yoke thickness has a negligible impact (sensitivity < 10% across all objectives). Hence, it is excluded from subsequent optimization, which focuses on the remaining three parameters.

4. 3D Finite Element Simulation

Next, a 3D FEA and optimization are conducted in detail on the three parameters of stator tooth width, PM width, and air-gap thickness. According to the Taguchi method, the experiment involves three factors, each with five levels. If a conventional orthogonal design, i.e., a full factorial experimental design, were to be used, it would require 5^3=125 experiments. The large number of experiments would lead to excessively high experimental costs and an impractically long duration. However, by employing the Taguchi method for orthogonal experiments and establishing an experimental matrix expressed as $L25(5^3)$, only 25 experiments are needed to achieve nearly the same effect as a full factorial experiment.

4.1. FEA Results

Based on the simulation experimental design planned in the previous section, the simulation utilizes the finite element solver of the software. The motor winding is configured with 40 turns with a wire diameter of 1 mm. When loaded, the effective value of the three-phase alternating current is 7.5 A, yielding a current density of J=9.55 A/mm^2. The experimental data are shown in Table 5.

4.2. Result Statistical Analysis

4.2.1. Factor Mean Effect Analysis

After obtaining the experimental results, the average value of the optimization objective at level j needs to be calculated. The formula for the average value is:

$$\bar{x}(j) = \frac{1}{n}\sum_{i=1}^{n} x_{j,i} \tag{1}$$

where j is the level value, n is the number of experiments at level j, and $x_{j,i}$ is the result of the i-th experiment at level j.

The mean values of the optimization objectives, thrust F_x, force ripple R_f, and thrust-to-mass ratio of the PM R_{fp} after separation, are shown in Table 6.

Fig. 6 illustrates the mean effect plots of individual factors on the optimization objectives and the degree of factor influence based on the data from Table 6.

4.2.2. Variance Analysis

Based on the mean value analysis from the previous section, the variance of each optimization objective at the five levels can be calculated. By analyzing the variance of the optimization objectives, the degree of influence of each factor on the optimization objectives can be determined.

The formula for variance calculation is:

$$S = \frac{1}{5}\sum_{i=1}^{5}[\bar{x}(i) - \bar{x}]^2 \tag{2}$$

Table 5. Experimental simulation data.

Experiment Number	w_s/mm	w_p/mm	t_g/mm	F_x/N	R_f/%	R_{fp}/N*kg^{-1}
1	6.5	2.0	0.35	149.44	18.86	1339
2	6.5	2.1	0.40	146.14	19.13	1247
3	6.5	2.2	0.45	143.40	19.81	1168
4	6.5	2.3	0.50	139.37	19.06	1086
5	6.5	2.4	0.55	137.14	18.82	1024
6	7.0	2.0	0.40	144.73	17.29	1297
7	7.0	2.1	0.45	141.54	17.59	1208
8	7.0	2.2	0.50	139.25	17.82	1134
9	7.0	2.3	0.55	135.42	18.06	1055
10	7.0	2.4	0.35	162.40	20.82	1212
11	7.5	2.0	0.45	139.15	17.93	1247
12	7.5	2.1	0.50	136.64	17.32	1166
13	7.5	2.2	0.55	134.46	17.28	1095
14	7.5	2.3	0.35	160.35	19.88	1249
15	7.5	2.4	0.40	156.90	19.77	1171
16	8.0	2.0	0.50	133.34	15.52	1194
17	8.0	2.1	0.55	131.06	16.08	1118
18	8.0	2.2	0.35	158.01	17.86	1287
19	8.0	2.3	0.40	153.65	18.00	1197
20	8.0	2.4	0.45	150.50	18.45	1123
21	8.5	2.0	0.55	127.39	18.09	1141
22	8.5	2.1	0.35	154.04	20.97	1314
23	8.5	2.2	0.40	150.75	20.60	1228
24	8.5	2.3	0.45	146.62	20.51	1142
25	8.5	2.4	0.50	144.09	19.73	1076

Table 6. Separated mean values of optimization objectives.

Factor	Level	F_x/N	R_f/%	R_{fp}/N*kg^{-1}
w_s	1	143.10	19.14	1173
	2	144.67	18.32	1182
	3	145.50	18.44	1186
	4	145.31	17.19	1184
	5	144.58	20.56	1181
w_p	1	138.81	18.12	1244
	2	141.88	18.22	1211
	3	145.17	18.68	1183
	4	147.08	19.11	1146
	5	150.20	19.52	1122
t_g	1	156.85	19.69	1281
	2	150.43	18.96	1228
	3	144.24	18.86	1178
	4	138.54	17.9	1132
	5	133.10	18.25	1087

Based on the data from Table 6 and Fig. 6, the variance of the three factors, stator tooth width w_s, PM width w_p, and air-gap thickness t_g, on the thrust F_x, force ripple R_f, and thrust-to-mass ratio of the PM R_{fp} are calculated, along with the proportion of the total variance they represent. The calculation results are shown in Table 7.

Table 7 reveals that air-gap thickness t_g is the greatest impact parameter for F_x, accounting for 81.08% of the total variance, and also significantly affects R_{fp} (70.79%). The stator tooth width w_s shows the strongest influence on R_f, contributing 64.95% of the total variance. As illustrated in Fig. 6, increasing t_g results in a decrease in both F_x and R_{fp}. Conversely, R_f initially decreases and then increases with increasing w_s, indicating a non-linear relationship and the potential for an optimal design point.

4.3. Comparison of Optimization Schemes

Based on the analysis in the previous section, four

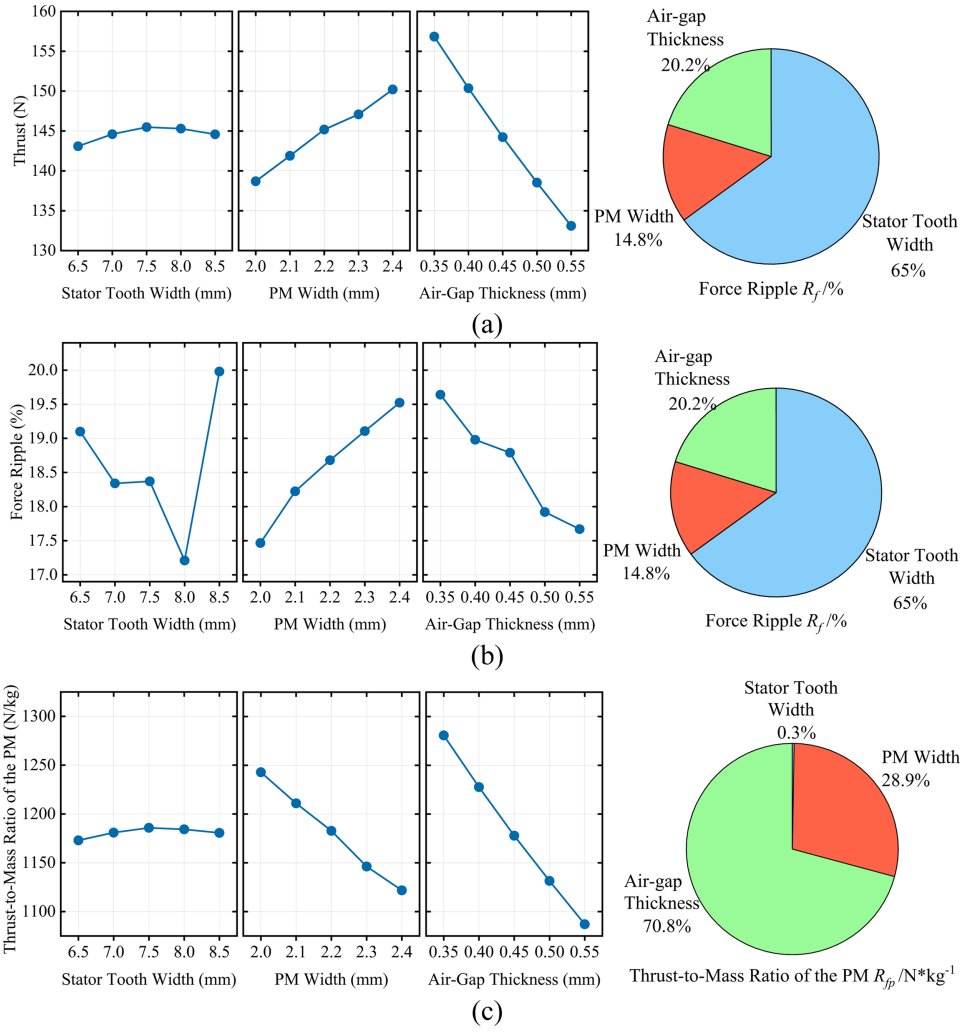

Fig. 6. (Color online) Main effect of design factors on optimization objectives and their contribution ratios. (a) Thrust. (b) Force ripple. (c) Thrust-to-mass ratio of the PM.

Table 7. Variance and proportion of variance for each factor.

Factor	F_x/N		R_f/%		R_{fp}/N*kg^{-1}	
	Variance	Proportion/%	Variance	Proportion/%	Variance	Proportion/%
w_s	0.7129	0.83	0.000123	64.95	4.3345	0.29
w_p	15.7646	18.09	0.000028	14.84	33.3755	28.91
t_g	70.6402	81.08	0.000038	20.21	29.5273	70.79

preliminary optimization schemes can be derived:

4.3.1. Maximum Thrust Expectation:

Based on Fig. 6(a), the air-gap thickness t_g has the most significant impact on thrust. It is set to 0.35 mm. The stator tooth width w_s and PM width w_p are set to 7.5 mm and 2.4 mm, respectively. Thus, the configuration is w_s (7.5), w_p (2.4), t_g (0.35).

4.3.2. Minimum Force Ripple Expectation:

Based on Fig. 6(b), the stator tooth width w_s has a significant impact on force ripple. It is set to 8.0 mm. The air-gap thickness t_g and PM width w_p are set to 0.55 mm and 2.0 mm, respectively. Thus, the configuration is w_s (8.0), w_p (2.0), t_g (0.55).

4.3.3. Maximum Thrust-to-Mass Ratio of the PM Expectation

Based on Fig. 6(c), the PM width w_p and air-gap thickness t_g are set to 2.0 mm and 0.35 mm, respectively. The stator tooth width w_s is set to 8.5 mm. Thus, the configuration is w_s (8.5), w_p (2.0), t_g (0.35).

4.3.4. Comprehensive Evaluation of Three Optimization Objectives:

The air-gap thickness t_g exerts the most significant influence on both thrust and the thrust-to-mass ratio of the PM, and is set to 0.35 mm. The stator tooth width w_s is most sensitive to force ripple and is set to 8.0 mm. The PM width w_p affects all three optimization objectives: it has a positive relationship with thrust and force ripple but a negative relationship with the thrust-to-mass ratio of the PM. To balance the optimization objectives, it is set to the intermediate value of 2.0 mm. Thus, the configuration is w_s (8.0), w_p (2.0), t_g (0.35).

Finite element simulations were conducted for these four schemes, and the results are shown in Table 8 above.

Based on the optimization of the three objectives—where higher thrust F_x and higher thrust-to-mass ratio of the PM R_{fp} are preferred, while lower force ripple R_f is preferred—an optimal function is defined as follows:

$$y = \left(\frac{F_x - F_{x\min}}{F_{x\max}} + \frac{R_{f\max} - R_f}{R_{f\max}} + \frac{R_{fp} - R_{fp\min}}{R_{fp\min}}\right)\times 100 \tag{3}$$

where $F_{x\min}$, $R_{f\max}$, and $R_{fp\min}$, are the minimum thrust F_x, maximum force ripple R_f, and minimum thrust-to-mass ratio of the PM R_{fp} from the experimental data in Table 5, which are 127.39 N, 20.98%, and 1024.18 N/kg, respectively. In addition, in the study, these three optimization objectives are crucial, so balanced weight coefficients are chosen, all set to 1.

The optimization effect of each scheme can be judged based on the value of y; the larger the y value, the better the optimization scheme. The optimal values for several optimization schemes are shown in Table 9.

From Table 9, it is evident that Scheme 4 has the best optimization effect, with an optimal function value reaching 72, which is higher than the other schemes. Additionally, to compare the effects of the four schemes before and after optimization, the optimal function assessment is also conducted for the initial 25 sets of Taguchi orthogonal experimental results, as shown in Table 10 below.

In Table 10, No. 0 represents the average objective function value (40.13) of 25 experimental sets, serving as the pre-optimization performance baseline. Optimized

Table 8. Optimal values for each scheme.

Scheme	F_x/N	R_f/%	R_{fp}/N*kg^{-1}
1	163.12	20.60	1218.19
2	127.87	15.39	1145.90
3	151.12	17.92	1354.23
4	151.94	16.83	1361.61

Table 9. Optimal values for each scheme.

Scheme	y
1	48.9
2	38.9
3	65.4
4	72.0

Table 10. Optimal values of Taguchi orthogonal experimental data.

Experiment Number	y	Experiment Number	y
1	58.1	14	53.1
2	45.3	15	43.3
3	32.2	15	47.3
4	24.6	17	35.4
5	17.9	18	64.6
6	57.8	19	51.7
7	45.2	20	39.9
8	35.1	21	25.2
9	23.2	22	49.3
10	46.6	23	40.1
11	45.5	24	28.9
12	38.5	25	24.1
13	30.1	0	40.13

schemes 1, 3, and 4 outperform this baseline, whereas scheme 2 falls below it and is therefore not an ideal optimization scheme. Among the experimental designs, No. 18 achieved the highest objective function value (64.6) and was selected as the original design for comparison. A detailed comparison between No. 18 and the optimized schemes is presented in Fig. 7.

As shown in Fig. 7(a), Scheme 1—optimized primarily for thrust—achieves the highest thrust of 163.1 N, a 3.2% improvement over the original design (No. 18). Fig. 7(b) shows that Scheme 2, designed to minimize for force ripple, reduces it to 15.4%, a 14% decrease compared to the original design. Scheme 3, targeting maximization of the thrust-to-mass ratio of the PM, achieves 1363.1 N/kg, representing a 5.89% increase.

Scheme 4, which aims to balance all three objectives, exhibits a 3.9% reduction in thrust of 151.9 N, but achieves significant improvements: force ripple is reduced by 6.1%, and the thrust-to-mass ratio of the PM increases by 5.8%. When comprehensively evaluated using the optimal function value y, Scheme 4 demonstrates the best overall performance in terms of multi-objective optimization.

Therefore, the optimized parameters for the motor are: w_s (8.0), w_p (2.0), t_g (0.35), which correspond to a stator tooth width of 8 mm, a PM width of 2 mm, and an air-gap thickness of 0.35 mm.

5. Conclusion

A 2DoFPM machine is designed in this paper, and multi-objective optimization and analysis of its linear component under the decoupling condition of the motor are conducted. The research results reveal the following:

1) The air-gap thickness significantly affects both the thrust and the thrust-to-mass ratio of the PM. The stator tooth width has the most distinct effect on the force ripple. Additionally, as air-gap thickness increases, both thrust and thrust-to-mass ratio of the PM decrease continuously. The influence of stator tooth width on force ripple first decreases and then increases as the tooth width increases.

2) Compared with the original design, Scheme 4 significantly improved overall performance and was therefore selected as the final parameter configuration for the motor.

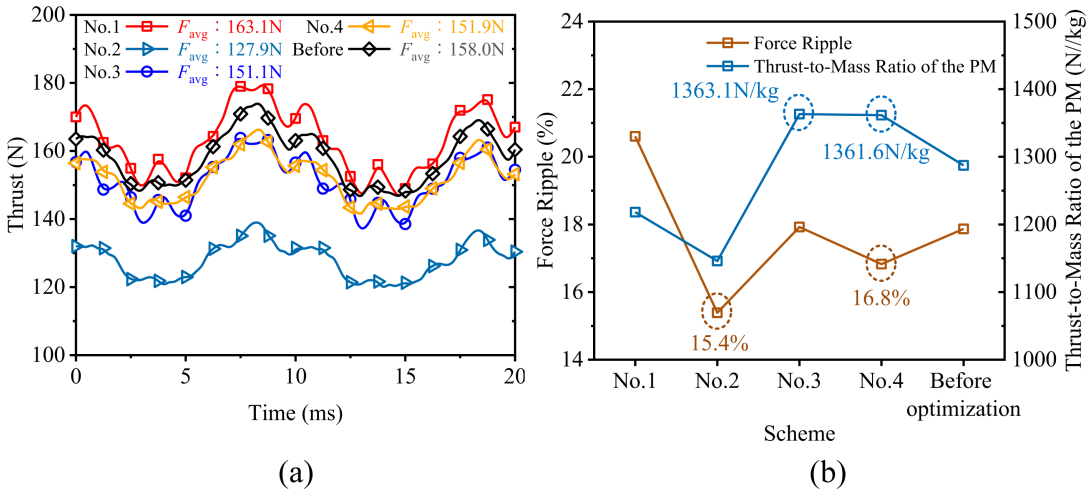

Fig. 7. (Color online) Comparison of the four optimized schemes with the original design. (a) Comparison of thrust. (b) Comparison of the force ripple and thrust-to-mass ratio of the PM.

The research in this paper provides a theoretical basis for the design and performance evaluation of the 2DoFPM machine and provides a theoretical and technical basis for subsequent in-depth analysis and further optimization of the integrated linear-rotary system.

Acknowledgments

This work was supported by the National Natural Science Foundation of China under Grant 52307070, the Natural Science Foundation of Henan under Grant 252300421095 and 252300421316, the National Natural Science Foundation of China under Grant 52277069, and 52207067, the Postdoctoral Fellowship Program of China Postdoctoral Science Foundation under Grant GZC20232386, the Major Special Project for Collaborative Innovation in Zhengzhou under Grant 20XTZX12023, and the Henan Province Science and Technology Research Project under Grant 252102221056.

References

[1] J. Si, L. Ai, H. Feng, Y. Zhu, and Y. Hu, 2014 17th International Conference on Electrical Machines and Systems (ICEMS), Hangzhou, China (2014) pp. 1157-1163.
[2] L. Xie, J. Si, Y. Hu, and Z. Wang, IEEE Transactions on Magnetics **55**, 1 (2019).
[3] J. Si, H. Feng, L. Ai, Y. Hu, and W. Cao, IEEE Transactions on Energy Conversion. **30**, 1200 (2015).
[4] E. Amiri, P. Gottipati, and E. A. Mendrela, 2011 1st International Conference on Electrical Energy Systems, Chennai, India (2011) pp. 203-206.
[5] L. Xie, J. Si, Y. Hu, H. Feng, and K. Ni, IEEE Transactions on Industrial Electronics. **67**, 931 (2020).
[6] P. Hekmati and I. P. Brown, IEEE Transactions on Magnetics. **54**, 1 (2018).
[7] Z. He, X. Cao, H. Chen, Z. Deng, Z. Hao, and R. Shi, IEEE Transactions on Industrial Electronics. **70**, 8757 (2023).
[8] S. Li, K. Cheng, N. Cheung, and Y. Zou, IEEE Transactions on Energy Conversion. **33**, 1363 (2018).
[9] S. Takanami, W. Kitagawa, and T. Takeshita, 2016 19th International Conference on Electrical Machines and Systems (ICEMS), Chiba, Japan (2016) pp. 1-6.
[10] P. Wang, H. Liang, J. Si, R. Nie, and S. Xu, 2024 27th International Conference on Electrical Machines and Systems (ICEMS), Fukuoka, Japan (2024) pp. 974-979.
[11] Y. He, Y. Zhou, and C. H. T. Lee, 2022 IEEE Energy Conversion Congress and Exposition (ECCE), Detroit, MI, USA (2022) pp. 1-7.
[12] L. Xu, M. Lin, X. Fu, X. Zhu, C. Zhang, and W. Wu, IEEE Transactions on Magnetics **53**, 11 (2017).
[13] J. Si, L. Zhang, and H. Feng, X. Xu, and X. Zhang, Journal of China Coal Society. **41**, 3167 (2016).
[14] J. Mu, B. Kou, and H. Zhang, 2023 26th International Conference on Electrical Machines and Systems (ICEMS), Zhuhai, China (2023) pp. 1404-1408.
[15] Z. Lan, X. Yang, and F. Wang, C. Zheng, Journal of Electrotechnical Technology **26**, 37 (2011).
[16] Y. Huang and T. Zhou, Journal of Electrotechnical Technology. **30**, 73 (2015).
[17] Y. Ye, L. Guo, and C. Lu, Journal of Electrical Engineering and Control **12**, 442 (2008).
[18] L. Li., Y. Tang, J. Liu, and D. Pan, Chinese Journal of Electrical Engineering, CSCD. **33**, 69 (2013).
[19] J. Wang, H. Li, Y. Zhou, J. Wang, L. Liu, and X. Wang, 2021 24th International Conference on Electrical Machines and Systems (ICEMS) (2021) pp. 1073-1078.
[20] B. Li, W. Xie, and X. Xiao, 2024 4th Power System and Green Energy Conference (PSGEC), Shanghai, China (2024) pp. 1270-1274.
[21] W. Hu, H. Sun, G. Li, Y. Li, and Z. Xue, 2023 6th International Conference on Electrical Engineering and Green Energy (CEEGE), Grimstad, Norway (2023) pp. 124-129.
[22] S. Gong, X. Yang, and L. Ji., Electric Power Automation Equipment. **32**, 60 (2012).
[23] P. Wang, W. Hua, G. Zhang, B. Wang, and M. Cheng, IEEE Transactions on Industrial Electronics. **63**, 2370 (2022).